Available online at www.sciencedirect.com
SCIENCE DIRECT®
International Journal of Heat and Mass Transfer 48 (2005) 293–305
International Journal of HEAT and MASS TRANSFER
www.elsevier.com/locate/ijhmt

The heat transfer limit of step-graded metal felt heat pipe wicks

Richard R. Williams, Daniel K. Harris *

Department of Mechanical Engineering, College of Engineering, Auburn University, 201 Ross Hall, Auburn, AL 36849-5341, USA

Received 17 October 2003; received in revised form 23 August 2004

Abstract

The heat transfer limit of two control metal fit wicks and two step-graded metal felt wicks was measured and compared to theoretical values. The wicks were planar and fabricated from 316 stainless steel. The working fluid was both water and methanol. The non-graded control wicks were measured to be at or near the wick's capillary heat transfer limit. The step-graded wicks failed much earlier than the theoretical capillary limit for each wick. Additional tests and analyses were conducted determining the failure to be caused from vapor formation within the step-graded wicks whereas the fine top layer trapped the vapor, resulting in failure.

1. Introduction

A heat pipe is an evaporation–condensation device for transferring heat in which the latent heat of vaporization is exploited to transport heat over long distances with a corresponding small temperature difference. The heat transport is realized by means of evaporating a liquid in the heat inlet region (called the evaporator) and subsequently condensing the vapor in a heat rejection region (called the condenser). Closed circulation of the working fluid is maintained by capillary action and/or bulk forces [1]. The heat pipe was originally invented by Gaugler [2] of the General Motors Corporation in 1944, but did not truly garner any significant attention within the heat transfer community until the space program resurrected the concept in the early 1960's. Early development of terrestrial applications of heat pipes proceeded slowly; however due to the high cost of energy, the industrial community has begun to appreciate the significance of heat pipes in energy savings and design improvements in various applications [3]. Most recently, with heat densities of electronic components continually increasing, there is a growing interest in using heat pipes for transferring and spreading heat in conjunction with cooling these components [4,5].

A simple constant conductance heat pipe consists of a sealed case lined with an annular porous wicking material. The wick is filled with a working fluid in the liquid state. A heat load is placed in contact with the casing at the evaporator end. Heat is transferred radially through the case and into the wick. This causes the liquid to evaporate, transferring mass from the wick to the vapor core. This addition of mass in the vapor core increases the pressure of the vapor at the evaporator end of the pipe, thus creating a pressure differential that drives vapor flow to the condenser end of the heat pipe. Heat is removed via a suitable heat sink attached to the outside of the casing at the condenser end. This causes the vapor to condense, replacing previously evaporated liquid mass to the wick. In the absence of bulk forces (gravity, centrifugal, etc) in the axial direction, capillary

* Corresponding author. Tel.: +1 334 844 3337; fax: +1 334 844 3307.
E-mail address: harridk@auburn.edu (D.K. Harris).

0017-9310/$ - see front matter © 2004 Elsevier Ltd. All rights reserved.
doi:10.1016/j.ijheatmasstransfer.2004.08.024

Nomenclature

A	cross-sectional area of wick
C_{cp}	conductance of the copper plate
C_w	conductance of the wick
g	gravitational acceleration
h_{fg}	enthalpy of vaporization
K	liquid permeability
K_1	liquid permeability of the top layer of the step-graded wick
K_2	liquid permeability of the bottom layer of the step-graded wick
k_{eff}	effective thermal conductivity of the wick
L	overall length of heat pipe
L_a	adiabatic length
L_c	condenser length
L_e	evaporator length
L_{eff}	effective length of the wick
$\dot{m}$	mass flow rate through the wick
$\dot{m}_1$	mass flow rate through the top layer of the step-graded wick
$\dot{m}_2$	mass flow rate through the bottom layer of the step-graded wick
P_l	liquid pressure
$P_{sat,pw}$	saturation pressure of a bubble located at the pipe–wick interface
P_v	pressure of the vapor
ΔP	pressure differential
ΔP_1	liquid pressure differential through the top layer of the step-graded wick
ΔP_2	liquid pressure differential through the bottom layer of the step-graded wick
ΔP_b	bulk forces differential pressure
ΔP_c	capillary differential pressure
ΔP_l	pressured differential of liquid
ΔP_v	vapor differential pressure
$\dot{Q}$	heat transfer rate
$\dot{Q}_1$	heat transfer rate across the top layer of the step-graded wick
$\dot{Q}_2$	heat transfer rate across the bottom layer of the step-graded wick
$\dot{Q}_{b,max}$	boiling heat transfer limit
$\dot{Q}_{cap,max}$	capillary heat transfer limit
$\dot{Q}_{cp}$	heat transfer rate conducted down the copper plate
$\dot{Q}_e$	heat transfer rate of the evaporator
$\dot{Q}_{net}$	net heat transfer rate through wick
$\dot{q}_e$	evaporator heat flux
R_n	thermal resistances, $n = 1 - 10$
r	radius of curvature of liquid–vapor meniscus
r_b	radius of a vapor bubble
r_{eff}	effective radius of the porous wick
r_n	radius of a vapor nucleus
r^*	critical radius or Lorenz radius
T_l	liquid temperature at the wall
T_{pw}	temperature of the liquid at the evaporator pipe–wick interface
T_{sat}	saturation temperature at the pressure of the liquid
T_v	temperature of the vapor
T_{wv}	temperature of the liquid at the evaporator wick–vapor interface
TC1	temperature of thermocouple located 0.127 cm from end of evaporator
TC2	temperature of thermocouple located 5.207 cm from end of evaporator
TC3	temperature of thermocouple located 7.747 cm from end of evaporator
TC4	temperature of thermocouple located 10.287 cm from end of evaporator
TC5	temperature of thermocouple located 15.367 cm from end of evaporator
TC6	temperature of thermocouple located 20.447 cm from end of evaporator
TC7	temperature of thermocouple located in vapor space of the evaporator
TC8	temperature of thermocouple located in vapor space of the condenser
ΔT	temperature differential
ΔT_{cp}	temperature drop across the effective length of the copper plate
t	thickness of wick
t_1	thickness of the top layer of the step-graded wick
t_2	thickness of the bottom layer of the step-graded wick
v_{fg}	specific volume change from liquid to vapor
w	width of the wick

Greek symbols

ε	porosity
ε_1	porosity of the top layer of step-graded wick
ε_2	porosity of the bottom layer of step-graded wick
ϕ	heat pipe tilt angle
μ	dynamic viscosity
ρ	density
ρ_v	density of the vapor
σ	surface tension
θ	wetting angle of liquid–solid–vapor interface

forces "pump" the liquid axially through the wick, feeding liquid back to the evaporator.

An advantage of a heat pipe over other conventional methods to transfer heat, such as a finned heat sink, is that a heat pipe can have an extremely high thermal conductance in steady state operation. Hence, a heat pipe can transfer a high amount of heat over a relatively long length with a comparatively small temperature differential. Heat pipes with liquid metal working fluids can have a thermal conductance of a thousand or even tens of thousands of times greater than the best solid metallic conductors, silver or copper [1]. Heat pipes, such as those studied in this work that utilize water as the working fluid, can have a thermal conductance tens of times greater than the best metallic conductors. This is because the heat transfer in a heat pipe utilizes the phase change of the working fluid, where a high amount of heat can be transferred with very little temperature difference between the source and sink.

There are generally at least five physical phenomena that will limit, and in some cases catastrophically limit, a heat pipe's ability to transfer heat. They are commonly known as the sonic limit, the capillary limit, the viscous limit, the entrainment limit, and the boiling limit [6].

The work of this study determined the impact of the wick on both the capillary and boiling limits within low temperature heat pipes utilizing water or methanol as the working fluid. The specific class of wicks studied are generically referred to as metal felts. Metal felts may have some unique advantages compared to other wick materials such as wire screens or packed powders. Specifically, wire screens and packed powders are generally restricted to a specific packing geometry such that the pore size and porosity (void volume fraction) and substrate characteristic length (diameter for spheres and wires) cannot be independently varied. Mono-diameter packed powders stably pack over a fairly narrow porosity range of 0.36–0.44 [7], regardless of powder diameter. Screens that use standard manufacturing techniques are limited to pore diameters down to about 40 μm (625 mesh) and porosity in the narrow range of about 0.6–0.7. Whereas metal felts can be manufactured with pore diameters down to about 10 μm over a porosity range of 0.1–0.95 or higher [8,9]. It was a hypothesis of this work that the heat transfer limit can be increased with the selection, engineering, and gradation of the pore structure (porosity, fiber diameter, pore diameter and pore diameter distribution) and geometry of the wick. This was accomplished by step-grading the wick to provide a high permeable base layer topped by a low effective radius top layer.

2. The capillary heat transfer limit

Chi [6] proposes a pressure balance amongst the wick and vapor core within the heat pipe as expressed in Eq. (1).

$$\Delta P_c = \Delta P_l + \Delta P_v + \Delta P_b \tag{1}$$

Similar to the analysis of Chi [6], except for a flat plat heat pipe in cartesian coordinates, and substituting the Young–Laplace equation for ΔP_c, Darcy's law for ΔP_l, hydrostatic pressure due to gravity for ΔP_b, and the steady state closed system energy equation to relate mass flow rate and heat transfer rate and re-arranging yields:

$$\dot{Q}_e = 2\left(\frac{KA}{rL_{eff}}\right)\left(\frac{h_{fg}\sigma\rho\cos(\theta)}{\mu}\right)\left(1 - \frac{r\rho gL\sin(\phi)}{2\sigma\cos(\theta)} - \Delta P_v\right) \tag{2}$$

The pressure drop of the vapor can be expressed using the appropriate correlation such as Hagen–Poiseuille flow for the geometry of the vapor space within the heat pipe. Chi, [6], and many others, define the effective wick length as $0.5L_e + L_a + 0.5L_c$.

Eq. (2) represents the heat transfer rate as a function of wick properties, represented by the first bracketed term, working fluid properties and its interaction with the wick's solid surface, represented by the second bracketed term, and the impact of bulk forces, represented by the third bracketed term. For a given wick, working fluid (assuming constant properties) and heat pipe orientation, Eq. (2) has one independent variable, r. As the heat transfer rate is increased, the capillary radius changes, becoming smaller as it adjusts to the increase pressure differential across the liquid–vapor interface. The radius adjusts until the surface tension can no longer support the pressure differential and the meniscus collapses. The failure normally happens at the far end of the evaporator first, drying out the wick from the evaporator towards the condenser. The failure causes a reduction in the heat transfer in the evaporator, driving up evaporator temperature and ultimately causes the heat pipe to stop functioning. Mechanistically, this phenomenon has been described in at least two ways. Silverstein [10] describes a failure mechanism in which vapor is forced into the wick, causing the wick to dry out, leading to large and rapid reduction in the ability to transfer heat into the evaporator. Pruzan et al. [11] describe a failure mechanism in which the capillary pressure is no longer sufficient to feed the evaporator, or in other words, the mass flow rate of vapor leaving the evaporator exceeds the mass flow rate of liquid feeding the evaporator, causing the evaporator to dry out. The evaporator dry out leads to large and rapid reduction in the ability to transfer heat into the evaporator. In either case, it is the wick that is limiting the heat transfer rate of the heat pipe. This limit on heat transfer is often called the capillary limit [1,6], hydrodynamic limit [3], wicking limit [10], or dry out heat flux [12].

The radius, r, that can support the maximum differential pressure across the liquid–vapor interface is often referred to as the effective radius, r_{eff}. The effective radius is a property of the wick and the method of the

determination of the value is described by Williams and Harris [13]. Setting r equal to r_{eff} in Eq. (2) yields an expression for the capillary heat transfer limit, $\dot{Q}_{\text{cap,max}}$:

$$\dot{Q}_{\text{cap,max}} = 2\left(\frac{KA}{r_{\text{eff}}L_{\text{eff}}}\right)\left(\frac{h_{\text{fg}}\sigma\rho\cos(\theta)}{\mu}\right) \times \left(1 - \frac{r_{\text{eff}}\rho g L\sin(\phi)}{2\sigma\cos(\theta)} - \Delta P_{\text{v}}\right) \quad (3)$$

The ability of a heat pipe to transfer heat can be limited by the properties of the wick. The wick's pore structure is a governing parameter in determining permeability and effective radius. The above analysis is based on the assumption of isotropic wick properties. It is postulated that the capillary limit is a function of the liquid permeability in the longitudinal (axial) direction and the effective radius in the transverse (normal) direction. Metal felt wicks may provide an additional degree of freedom, possibly allowing for high longitudinal permeability while achieving a low effective pore radius in the transverse direction. In particular, engineering the pore structure for anisotropic wick properties and/or grading the porosity in the transverse direction may allow for achieving a wick structure that has an increase in the ratio of K/r_{eff}, thus increasing the capillary limit per Eq. (3). This increase in the ratio of K/r_{eff} may also allow for a decrease in wick thickness t, thus lowering the heat transfer resistance, and hence, the operating temperature.

2.1. The boiling heat transfer limit

The primary mechanism of the heat transfer within the evaporator of the heat pipe is evaporation of the liquid at the liquid–vapor interface [6]. Fig. 1 is a diagram of the wick geometry, temperatures and pressures in the evaporator of a flat plate heat pipe. The wick is shown as evenly spaced spheres for illustrative purposes, but could be any substrate with any packing arrangement. It is further assumed that there is some intimate contact of the substrate particles with adjacent substrate particles.

Dunn and Reay, [14], among others, propose a simple conduction model using Fourier's Law for the heat transfer from the heat pipe wall to the surface of the wick. This can be expressed in rectangular coordinates as:

$$\dot{Q}_{\text{e}} = \frac{k_{\text{eff}}L_{\text{e}}w}{t}(T_{\text{pw}} - T_{\text{wv}}) \quad (4)$$

Eq. (4) can also be expressed in terms of evaporator heat flux $\dot{q}_{\text{e}}$, by dividing through by the area normal to heat transfer, L_{e} times w, yielding:

$$\dot{q}_{\text{e}} = \frac{k_{\text{eff}}}{t}(T_{\text{pw}} - T_{\text{wv}}) \quad (5)$$

Eq. (5) yields some interesting insight. Evaporator heat flux can be increased by increasing the effective thermal conductivity of the wick or by decreasing the thickness of the wick. The effective thermal conductivity of various wick structures has been studied fairly extensively [3,15,16]. In general, the correlations that have been developed are some combination of the thermal conductivity of the substrate, the thermal conductivity of the fluid within the wick, and the porosity of the wick. These correlations vary with the type of porous media and the effective thermal conductivity is certainly a function of pore structure. In other words, for metal wicks with non-metal or low thermal conductivity working fluids, the more intimate contact within the wick structure, the more thermally conductive the wick.

For a given wick design and working fluid, both k_{eff} and t are fixed; therefore, the evaporator heat flux varies directly with the temperature difference of the liquid across the thickness of the wick. At low heat fluxes, many investigators [17–19] have observed the linear relationship between heat flux and temperature difference. However at high heat fluxes, the mechanism of heat transfer changes, sometimes increasing, but ultimately decreasing the effective heat transfer coefficient, and limiting the heat flux that a given design can sustain. The mechanism often described that causes the decrease in the heat transfer coefficient is the nucleation of bubbles within the wick structure followed by a trapping of

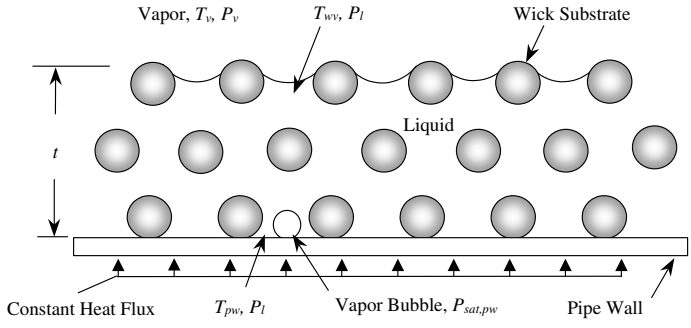

Fig. 1. Wick bubble nucleation.

vapor at the pipe wall. The vapor essentially insulates the wall from the liquid, increasing the resistance to heat flow, leading to high wall temperatures if heat flux is maintained at the high value. This is similar to critical heat flux that is observed in pool boiling [20]. The heat flux corresponding to the heat flux at which marks the onset of nucleation is known as the heat pipe's boiling heat transfer limit.

The analysis of the boiling limit involves the theory of bubble nucleation and growth. The development of a heat pipe's boiling heat transfer limit is attributed to Chi [6], except Chi's analysis has been modified for a flat plate heat pipe in cartesion coordinates. The analysis yields and expression for the heat transfer rate of the evaporator required to support a nucleate bubble as:

$$\dot{Q}_e = \frac{k_{eff} L_e w}{t} \frac{T_v}{h_{fg}\rho_v} \left(\frac{2\sigma}{r_b} - \Delta P_c \right) \tag{6}$$

Nucleation theory dictates that there is a minimum value for the initial radius of the vapor bubble [21]. This is dependent upon fluid properties and surface conditions. If the radius of the vapor bubble is smaller than the radius required to sustain bubble growth, the vapor bubble will collapse. If the radius is larger than the radius required to sustain growth, the bubble will grow. Setting the r_b equal to the bubble radius required to sustain nucleation, r_n, yields an equation in which the heat flux is just large enough for nucleation. Now assuming all nucleation is detrimental to the heat transfer performance, or, at the onset of nucleation the wick of the heat pipe rapidly becomes filled with vapor, the following relationship is developed for the boiling limit, $\dot{Q}_{b,max}$:

$$\dot{Q}_{b,max} = \frac{k_{eff} L_e w}{t} \frac{T_v}{h_{fg}\rho_v} \left(\frac{2\sigma}{r_n} - \Delta P_c \right) \tag{7}$$

Chi [6] recommends conservatively using a value on the order of 0.25–25 μm for r_n for heat pipes that use copper wicks and water as the working fluid (also called copper water heat pipes). If the working fluid is clean and degassed and the heat pipe internals are very clean, a value on the order of 0.025 to 0.25 μm can be used [6]. The theory of Lorenz [22] predicts that the larger nucleation sites are the first to become active; therefore, conservatively the highest value of r_n should be chosen. Alternately, the theory of Lorenz [22] could be used to directly calculate the appropriate value. In any case, the boiling limit as described by Eq. (7) can be increased by taking steps such as degassing and cleaning to lower the value of r_n.

Some investigators have observed an improvement in heat transfer at the onset of bubble formation [23,24]. These works suggest that some wick structures can support some level of nucleate boiling prior to reaching the boiling heat transfer limit. In these studies, the heat transfer rate is measured to be higher than that predicted by evaporation alone, further supporting the mechanism of simultaneous evaporation and nucleate boiling heat transfer.

3. Step-graded wick description

Twelve screening samples of metal felts were initially evaluated for bulk porosity, in-plane and cross-plane effective radius, and in-plane and cross-plane liquid permeability as reported in Williams and Harris [13]. The wicks used within the present work were selected from these twelve screening samples. Two sets of wicks were evaluated in the present work. Each set consisted of an un-graded control and a step-graded wick. The step-graded wicks were fabricated with a high permeability base layer against the pipe wall and a low effective radius top layer against the vapor space. The properties of the step-graded wick were approximated as one dimensional fluid and heat flow within the wick. This approach is adequate since only the bulk-mass averaged properties were being sought. Additionally, this approximation has been used by other investigators for the analysis of composite wick performance [3,14].

3.1. Bulk porosity

The porosity of the step-graded wick was calculated from the individual porosities and volumes with the following equation:

$$\varepsilon = \frac{\varepsilon_1 t_1 + \varepsilon_2 t_2}{t} \tag{8}$$

3.2. Cross-plane effective radius

The purpose of step-grading was to provide a wick with a small cross-plane effective radius at the liquid vapor interface while providing a highly permeable base layer for longitudinal flow of the liquid as it is transported from the condenser to the evaporator. The cross-plane effective radius was taken to be identical to the cross-plane effective radius of the top layer.

3.3. In-plane liquid permeability

The in-plane liquid permeability of the step-graded wick was calculated by modeling the wick as two parallel flow paths as defined by t_1, K_1 and t_2, K_2. The mass flow rate through the wick is the sum of the mass flow rate through each individual flow path, yielding:

$$\dot{m} = \dot{m}_1 + \dot{m}_2 \tag{9}$$

Expressing Darcy's Law in terms of mass flow rate and substituting into Eq. (9) yields:

$$\frac{\Delta PK\rho tw}{\mu L} = \frac{\Delta P_1 K_1 \rho t_1 w}{\mu L} + \frac{\Delta P_2 K_2 \rho t_2 w}{\mu L} \tag{10}$$

Recognizing that the mass flow rate will balance such that the pressure drop across each flow path is identical, or $\Delta P = \Delta P_1 = \Delta P_2$, eliminating the other like terms in Eq. (10), and then rearranging, yields an expression for the in-plane permeability of a step-graded wick in terms of the geometry and permeability of the two layers:

$$K = \frac{K_1 t_1 + K_2 t_2}{t} \tag{11}$$

3.4. Graded wick property measurements

The two graded wicks and two corresponding non-graded base layers for use as controls were manufactured by Technetics, Inc. and are described in Table 1. Graded wick A (Graded A) was manufactured with a base of screening sample 4A and a top of screening sample 3A. Control wick A (Control A) was manufactured with a base of screening sample 4A only. Graded wick B (Graded B) was manufactured with a base of screening sample 4B and a top of screening sample 3B. Control wick B (Control B) was manufactured with a base of screening sample 4B only. These wicks were then measured for porosity, cross-plane effective radius, and in-plane permeability using the techniques described in Williams and Harris [13]. The results of the measurements along with the theoretical values as calculated from Eqs. (8) and (11) are also shown in Table 1. The properties used to calculate the theoretical values were based on the measurements of the corresponding screening sample. There was good agreement between the theoretical and measured valve for both Control A and Graded A with the exception of cross-plane r_{eff} for the control wick. There was not was good agreement between the theoretical and measured valve for both Control B and Graded B. It was also believed that the thickness (when compared to the screening samples) of these wicks was not sufficient to establish homogeneity in the packing. In any case, the actual measured values were used to calculate the heat transfer limits within this study.

4. Wick heat transfer limit measurements

Many investigators study wick performance by building actual heat pipes and subjecting them to heat loads while measuring external temperatures. This method has the advantage of simplicity, but is limited by that which can be inferred from the external measurements, making it difficult to distinguish between cause and effect. Several investigators have attempted to improve upon the external measurements by placing the wick in an environmentally controlled test chamber. Some methods tested include Pruzan et al. [12], Noda et al. [25], and McCreery [26].

Fig. 2 is a schematic illustration of the wick test stand designed and utilized within this work [27]. It consisted of a copper wick mounting plate to which a test wick was mechanically clamped. A coarse (4 mesh) stainless steel screen was utilized to ensure the wick was held against the wick mounting plate. Thermally conductive epoxy was used to attach two Kapton heaters to the copper plate at the evaporator end to provide the heat source. A recirculating water chiller provided cooling at the condenser end of the plate. This was accomplished by cooling channels that were drilled into the copper plate. Twelve holes were drilled into the side of the plate for the insertion of Type E thermocouples. Small, 0.25 mm diameter thermocouples were potted into the holes utilizing a thermally conductive epoxy. The wick mounting plate was made as thin as possible in the evaporator and adiabatic section in order to minimize thermal conduction down the length of the plate, while still maintaining enough thickness for structural stability. The mounting plate's surface was treated using the oxidation process per [28]. Surface treatments such as this are often used in heat pipes to improve the wettability of the pipe and wick materials [14].

The wick mounting block and insulation block were place inside a vacuum chamber that consisted of a vacuum tee, a thermocouple feed through, a power feed

Table 1
Step-graded sample measurements

Sample	Thickness (mm) total/top	Theoretical			Measured		
		ε	Cross-plane r_{eff} (μm)	In-plane K (μm^2)	ε	Cross-plane r_{eff} (μm)	In-plane K (μm^2)
Control A	0.43/0.0	0.85	190	891	0.85	500	859
Graded A	0.63/0.20	0.86	28	619	0.87	44	792
Control B	0.53/0.0	0.74	93	151	0.79	211	391
Graded B	0.71/0.18	0.74	12.6	115	0.81	35	170

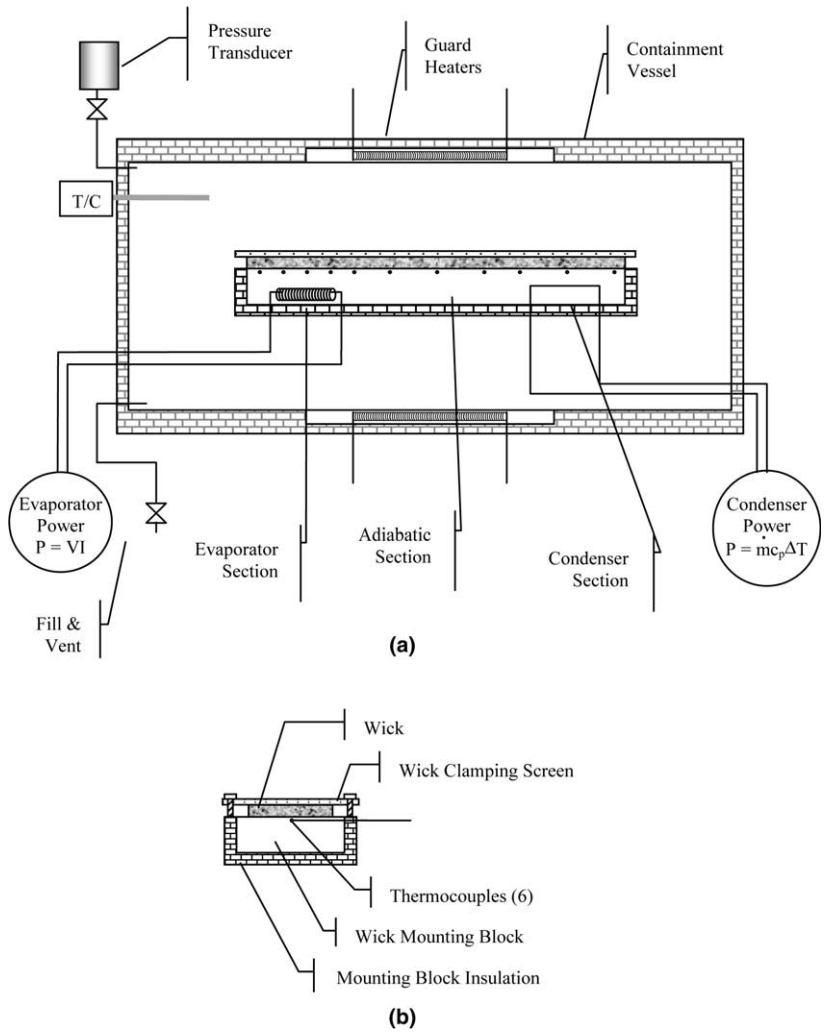

Fig. 2. Schematic of wick test stand: (a) side view, (b) end view.

through, a chill water, fill and vent, and pressure transducer feed through, and a Pyrex globe. The evaporator end of the wick was positioned such that it was visible through the cylindrical Pyrex globe. Guard heaters and external insulation were utilized to account for parasitic heat losses.

The wick test stand of the present work has several advantages of those described in the open literature [12,25,26]. First, the wick test stand could be operated in any orientation with respect to the gravity plane. Second, the wick test stand was readily adaptable for flow visualization studies of the evaporator region. Third, the wick test stand was well instrumented to record axial temperature profiles and account for parasitic heat losses. Forth, it isolated the wick from other vapor core specific phenomena, such as the vapor phase pressure drop and sonic limit, which are influenced by the heat pipe geometry and not wick properties. Finally, the wick test stand was easily compatible with wide range wick types and thickness and most low temperature working fluids.

4.1. Wick performance measurement procedure

The wick test stand and wicks were thoroughly cleaned. Upon installation of the wicks, the system was leak checked, leveled, and filled with degassed working fluid. The system was overfilled with approximately 100 ml of liquid. To ensure that the system was not limited by the ability to condense the fluid at rate sufficient to feed the evaporation, the temperature set point of the guard heaters was adjusted as necessary to maintain the condenser heat load as measured by the calorimeter to approximately 0.25 W greater than the evaporator input power as measured by the power supplies. This essentially operates the heat pipe in a slightly overfilled condition with respect to the wick volume. This is a

common operating condition of actual heat pipes [10]. The temperature set point of the guard heaters was determined to have a negligible effect on the temperature distribution within the wick base plate.

All tests were completed with the chiller at a set point of 20 °C. This provided an average condenser temperature as measured by TC6 of about 21 °C. After the establishment of the condenser power to a value above the first evaporator power set point (normally 2 or 3 W), the heater power was set. Each heater was operated at the same power level to provide the total evaporator heat load. The temperatures were monitored until steady state was achieved. Two minutes of temperature data were averaged to determine the steady state value. Normally, two sets of data were recorded about 5 min apart. Once the data was recorded at the given power level, the guard heater set point was raised and the test was repeated at the next power level. This procedure was repeated until failure was observed as indicated by a marked increase in the end temperature of the evaporator, TC1. In most cases, several more power increases were made to collect additional data. Visual observations were made and recorded at each power level by inspecting the wick using a low power (10× or 20×) binocular microscope. Upon completion of the test in the horizontal orientation, the system was allowed to cool back to steady state while the tilt angle was changed to the adverse tilt condition. The test was then repeated in the adverse tilt condition.

4.2. Wick heat transfer limit data reduction

The thermal system of the wick test stand was modeled by the resistance network illustrated in Fig. 3. The temperatures labeled on Fig. 3 correspond to those measured in the wick test stand. The average evaporator temperature was taken to be the mean of TC1 and TC2.

Neglecting the fact that the system was operated with a slight bias with respect to the condensation rate, a steady state heat balance yields:

$$\dot{Q}_{\text{net}} = \dot{Q}_{\text{e}} - \dot{Q}_{\text{cp}} \tag{12}$$

The conducted heat load through the copper plate can also be expressed as:

$$\dot{Q}_{\text{cp}} = C_{\text{cp}} \Delta T_{\text{cp}} \tag{13}$$

where $\Delta T_{\text{cp}} = ((\text{TC1} + \text{TC2})/2 - \text{TC6})$ is the temperature drop across the effective length of the plate. The copper plate conductance was empirically determined by operating the wick test stand evacuated and filled, but with no wick. The temperature difference of Eq. (13) was measured as a function of heat load. A least squares fit of the data to a line provided the slope, or C_{cp}, to be 0.31 W/°C. Combining Eqs. (12) and (13) and substituting the value for C_{cp} yields an expression for the net heat transfer rate through the wick as a function of measured values to be:

$$\dot{Q}_{\text{net}} = \dot{Q}_{\text{e}} - 0.31 \Delta T_{\text{cp}} \tag{14}$$

The net heat transfer rate through the wick can be expressed as:

$$\dot{Q}_{\text{net}} = \frac{\Delta T_{\text{cp}}}{\sum_{n=2}^{8} R_n} \tag{15}$$

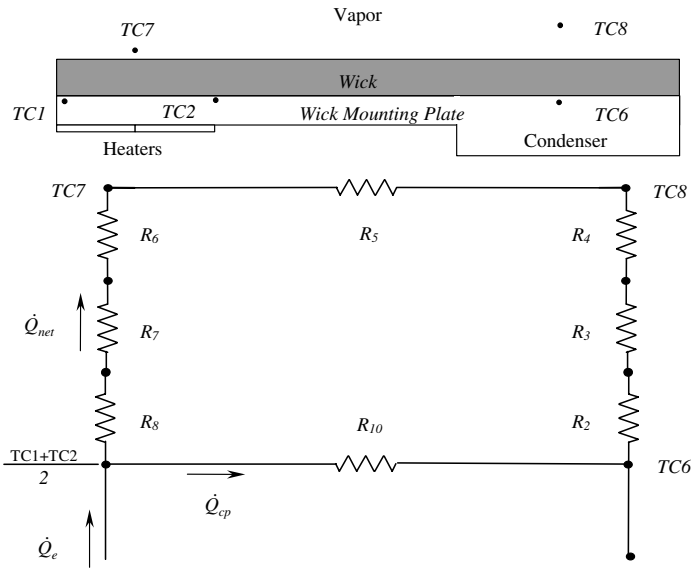

Fig. 3. Wick test stand thermal network.

The resistances across the liquid–vapor interface, R_4 and R_6, were small and generally can be ignored [6]. Additionally, the resistance of the copper plate, R_2 and R_8 were negligibly small due to the location of TC1, TC2, and TC6, and the high thermal conductivity of the copper. The resistance of the vapor, R_5, was also negligibly small due to the large vapor space. Neglecting all the negligible resistances and rearranging Eq. (15) yields and expression for the wick's conductance as:

$$C_w = \frac{\dot{Q}_{net}}{\Delta T_{cp}} \tag{16}$$

where $C_w = (R_3 + R_7)^{-1}$.

5. Experiment results and discussion

The two control wicks and two graded wicks were tested to determine the conductance and heat transfer limit of the wicks. Each wick was tested in the horizontal orientation and with an adverse tilt (evaporator higher than the condenser) of 3°. Water was initially used as the working fluid, however there was difficulty in re-wetting the Graded A wick upon its initial dryout. It was determined that the water was not as wetting as originally assumed. The wetting angle of water on the stainless steel wick was subsequently measured to be 70° using a sessile drop and an optical comparator similar to the technique described by Adamson [29]. This resulted in using methanol for the complete test. Both the partial results with water as the working fluid and the full results with methanol as the working fluid are presented below.

A simple method to compare the results of performance of each wick was to plot the net heat transfer rate of the wick, $\dot{Q}_{net}$, versus temperature difference between the evaporator and condenser, ΔT_{cp}. Fig. 4 illustrates the performance for a typical control and graded wick. Table 2 lists the average measured conductance of each wick with both working fluids. The average measured conductance was the mean value of the measurements, but did not include any data from the region of marked improvement through failure.

As illustrated in Fig. 4, the conductance (as indicated by the slope) was not measured to be constant, especially for the control wicks. The general trend in these wicks was an improvement, and in some cases a marked improvement in conductance as the heat transfer rate was increased. This marked increase in the heat transfer rate actually resulted in a drop in temperature with increased heat transfer rate as illustrated in Fig. 4. This phenomenon was also noted by Mighal and Plumb [30]. In their work, using R-11 as the working fluid at atmospheric pressure, they postulated that some nucleate boiling occurred at superheat values (the difference between plate temperature and saturation temperature in the evaporator) as low as 1 °C, resulting in an increase in the conductance. Then, when sufficient superheat exists (about 6 °C in [30]), Mighal and Plumb [30] postulated that nucleation was initiated over the entire wick, resulting in a marked temperature drop. This is similar to the overshoot commonly observed at the incipience of nucleation in pool boiling. Although not shown in the steady state data of Fig. 4(b), the indication of incipience was noted in transient data for the graded wicks, indicating an unstable operating condition. As the heat transfer rate was further increased, a

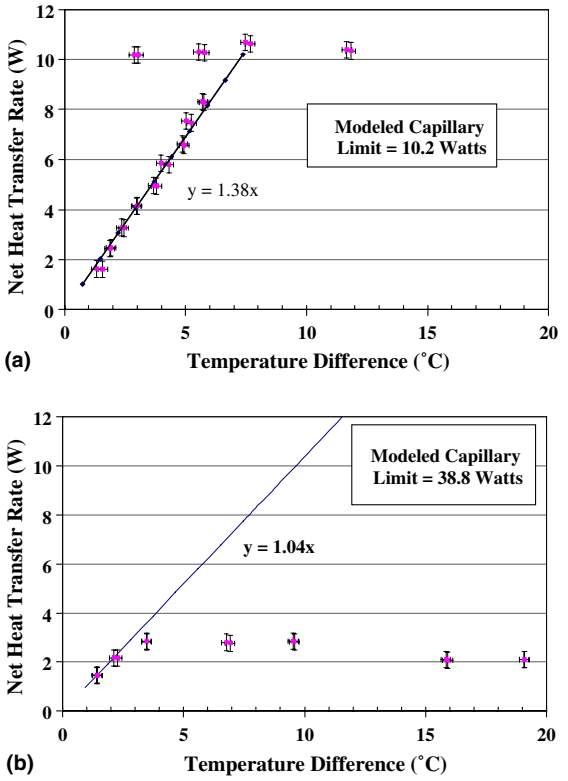

Fig. 4. Net heat transfer rate versus temperature difference, methanol, horizontal: (a) base B, (b) graded B.

Table 2
Average measured and modeled conductance, error ± 10%

Wick/fluid	Average measured conductance (W/°C)
Control A/water	4.6
Graded A/water	2.7
Control B/water	3.6
Control A/methanol	1.4
Graded A/methanol	2.1
Control B/methanol	1.4
Graded B/methanol	0.9

Table 3
Comparison of measured heat transfer limit and modeled capillary limit

Wick/fluid/angle	Measured heat transfer limit (W)	Modeled capillary limit (Eq. (3)) (W)	Modeled % difference
Control A/water/0	26.7 ± 1	13.5 ± 7.7	−49.4
Control A/water/3	15.1 ± 1	0 ± 3.1	−100
Graded A/water/0	11.5 ± 1	364 ± 192	3065
Control B/water/0	22.1 ± 1	18.3 ± 9.8	−17.2
Control B/water/3	18.8 ± 1	8.0 ± 9.0	−57.4
Control A/methanol/0	6.3 ± 0.5	7.5 ± 2.2	19.0
Control A/methanol/3	4.2 ± 0.5	0 ± 0.7	−100
Graded A/methanol/0	4.2 ± 0.5	132 ± 29	3040
Graded A/methanol/3	3.3 ± 0.5	116 ± 27	3415
Control B/methanol/0	10.3 ± 0.5	10.2 ± 2.4	−1.0
Control B/methanol/3	5.6 ± 0.5	5.2 ± 1.7	−7.1
Graded B/methanol/0	2.8 ± 0.5	38.8 ± 8.6	1285
Graded B/methanol/3	2.2 ± 0.5	35.1 ± 8.0	1495

marked increase in surface temperature was observed in both the present work and by Mughal and Plumb [30]. It was postulated in [30] that this was due a vapor film blanketing the surface of the wick mounting plate. The heat transfer rate at which the temperature was observed to increase was taken to be the wick's heat transfer limit. Table 3 list each the measured heat transfer limit of each wick and the capillary limit as calculated from Eq. (3).

The capillary or boiling heat transfer limits of a heat pipe are normally determined by incrementing the evaporator heat load while measuring the external surface temperature of the end of the evaporator as was the method employed by Noda et al. [25] and Moss and Kelly [31]. When a marked increase in this temperature was observed, the dry out of the wick is assumed to have occurred and the heat transfer rate was deemed the limit. In the case in which the wick is fully enclosed in an operable heat pipe, such as in [32], the actual failure mechanism cannot easily be determined and is often taken to be the capillary limit. In the present work, it was originally assumed that boiling would not occur within the wick at the operating conditions of the experiment, and the heat transfer limit would be the capillary limit. However, the results illustrated Table 3 challenged the validity of that assumption. Specifically, heat transfer limit of the graded wicks was measured to be more than an order of magnitude less than the capillary limit predicted by the model, while there was good agreement for the control wicks. The measured heat transfer limit was based on the average value of the net heat transfer just prior to failure and the value when failure was detected. The uncertainty placed on the measured heat transfer limit accounts for the fact that the net heat transfer rate at failure was not specifically measured. The uncertainty is higher for the water compared to methanol due to the fact that total power was incremented at a higher step. The larger uncertainty for the modeled capillary limit of water is primarily driven by a large sensitivity to the wetting angle at high wetting angles.

Table 3 shows that the measured heat transfer limit and the modeled capillary limit fit fairly well for the control wicks. Assuming the measured heat transfer limit was indeed the capillary limit, there was a tendency of the model to under-predict the capillary limit, especially with adverse tilt conditions. The model's under-prediction of the capillary limit may be explained by the non-homogeneous nature of the base wicks, especially Control A. The wick was characterized by an r_{eff} of 500 μm; however there were many smaller interconnected pores within the wick. When operated at the adverse tilt, it was visually observed that initially only the largest pores drained, and most of the wick still supported liquid, whereas the model assumes the entire wick would drain. This effect was less pronounced with the more homogeneous Control B wick.

Conversely, Table 3 shows that the measured heat transfer limit and the modeled capillary limit do not fit well for the graded wicks. Three hypotheses were proposed and investigated to explain the cause of the failure. The first hypothesis was that the wick was not well sealed, resulting in an exposed pore much greater in size than the measured r_{eff}, causing a premature capillary heat transfer limit failure. The second hypothesis was that liquid receded into the graded top layer of the wick, resulting in significant vapor flow through this layer, causing an unaccounted for vapor pressure drop and a premature capillary heat transfer limit failure. The third hypothesis was that nucleate boiling occurred within the wick, resulting in a boiling heat transfer limit failure.

The first two hypotheses were tested and determined not to be the likely cause of the low heat transfer limit [27]. The analysis of the nucleate boiling hypothesis is reported below.

5.1. Analysis of nucleate boiling hypothesis

The underlying assumption that was made prior to wick testing was that no nucleate boiling would occur if the nucleation radius, r_n, was small, and the wick was thin, such that the amount of evaporator wall superheat was kept to a minimum. Unfortunately, within the open literature, the appropriate range of values of r_n for a given wick structure is both unreliable and contradictory [17]. However, it is clear that if vapor were to form within the base structure of an edge-sealed wick, it would rapidly displace the liquid and result in a failure of the heat pipe. Several additional experiments and analyses were conducted to test the hypothesis that nucleate boiling or vapor formation within the wick structure was the cause of the heat transfer limit failure.

The heterogeneous nucleation of vapor bubbles on a surface was studied by Lorenz et al. [22]. The nucleation requires a site or cavity to initiate and sustain bubble growth. Lorenz et al. [22] determined that a given somewhat idealized cavity would be active if its radius r_n, is greater than a critical radius, called the Lorenz radius or r^* given by:

$$r^* = \frac{2\sigma T_{sat} v_{fg}}{h_{fg}(T_l - T_{sat})} \tag{17}$$

In the evaporator of a heat pipe, T_{sat} was taken to be the vapor temperature, T_v. Assuming the nucleation occurs at the wick pipe wall interface, $(T_l - T_{sat})$ was the amount of liquid superheat or simply the temperature drop across the wick in the direction normal to the heat transfer.

Eq. (17) can be used to calculate the r^* for given operating conditions of a heat pipe, such that if there are sites characterized by a radius $r_n > r^*$, nucleation will occur. Without the ability to measure r_n within a wick, it was difficult to determine if conditions for nucleation existed. However, making the assumption that the measured heat transfer limit as shown on Table 3 was a result of the activation of sites characterized by the radius, r_n, the value of r_n was calculated by using the model FLATPIPE [27] by iterating Eq. (7) on r_n until $\dot{Q}_{b,max}$ equaled the measured heat transfer limit. For that particular condition of fluid properties and liquid superheat, r^* was calculated. Fig. 5 is a graph of r_n versus r^* for all wicks, both working fluids, and both tilt angles. The calculated points that fall above the line $r_n = r^*$ were predicted to be active sites. The two points that fall in the shaded area below the line $r_n = r^*$ were predicted not to be active. These two wicks were Controls A and B with water at a 3° adverse tilt. All graded wicks with both fluids were predicted to have active nucleation sites by this analysis. Additionally, the amount of liquid superheat present at the point of failure was predicted to be very low, on the order of 1–5 °C. The observed level of superheat is consistent with the data presented by both Afgan et al. [33] and Rosenfeld [23], where vapor formation was observed at superheats as low a 1.0 °C in water and methylamine, respectively.

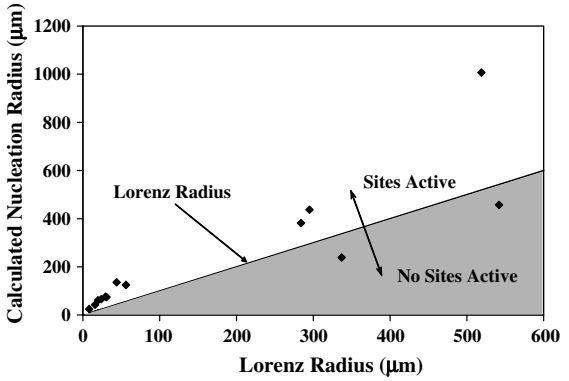

Fig. 5. Calculated nucleation radius versus Lorenz radius.

The mechanism of nucleate boiling causing dryout of the graded wicks due to inability of vapor to escape was additionally tested by the evaluation of wick Graded B with methanol, but without sealing the edges of the wick. It was postulated that there would be improved performance compared to the sealed wick, as vapor would be allowed to escape from the edges. The expected overall gain in the capillary limit vanishes without the edges sealed, but this allowed the hypothesis to be further tested.

Comparing results of an unsealed wick to those found in Fig. 4(b), there was a marked improvement in both the measured conductance and the heat transfer limit of the non-sealed wick compared to the sealed wick. The measured conductance increased by a factor of 1.5 while the heat transfer limit increased by a factor of 2.5. Additionally it was noted that the failure was measured to be more gradual rather than sudden.

These observations were supported by the work of Mughal and Plumb [30]. In their work, they added grooves to the base of foam metal wicks to provide paths for the vapor to escape and measured an increase in both the conductance and heat transfer limit as grooves were added. They also noted the more gradual failure with the presence of the grooves.

The analyses and observations presented above all support the formation of vapor within the wick as the source of the low heat transfer limit of the graded wicks.

6. Conclusions

The heat transfer limit of the step-graded metal felt wicks was measured to an order of magnitude lower than the capillary limit for these wicks. Three hypotheses were proposed and evaluated for the cause of the low measured heat transfer limit of the graded wicks. The mechanisms of a leak in the edge seal and vapor pressure drop due to liquid recession were found not to be the cause of the premature failures. The mechanism of nucleate boiling or vapor formation was determined to be the cause of the failure. It was apparent from the analyses, that vapor formation was likely to exist in all the wicks; however the control wicks were tolerant to the presence of vapor. It is not evident that the failure of the control wicks was due exclusively to either the capillary limit or the boiling limit. However, the vapor formation that occurred in the graded wicks not only reduced the conductance of these wicks, but ultimately reduced the heat transfer limit by an order of magnitude compared the to expected value. Leaving the edges open made the graded wick more tolerant to vapor formation and improved the conductance and heat transfer limit,

however, the heat transfer limit still fell well short of the expected value.

The level of gradation used in this work was aggressive, creating an intolerable resistance for vapor to escape from the wick. Additional work is proposed to determine if less aggressive gradation will provide an improvement to the capillary limit while still allowing vapor to escape, thus providing an overall increase in the wick's heat transfer limit.

Acknowledgments

This work was performed under a US Army contract at Auburn University administered through the US Army Space and Missile Defense Command. Sincere appreciation is also expressed to Technetics Corporation of DeLand, FL. for supplying the metal felt samples tested during this program.

References

[1] M.N. Ivanovskii, V.P. Sorokin, I.V. Yagodkin, The Physical Principles of Heat Pipes, Clarendon Press Oxford, New York, 1982, Chapter 1.
[2] R. Gaugler, US Patent No. 2350348, 1944.
[3] A. Faghri, Heat Pipe Science and Technology, Taylor and Francis, Washington, DC, 1995, chapters 1 and 3.
[4] B. Palm, N. Tengblad, Cooling of electronics by heat pipes and thermosyphons—a review of methods and possibilities, in: Proceedings of the 1996 31st ASME National Heat Transfer Conference, Part 7 (of 8), Sponsored by: ASME, ASME, NY, 1996, pp. 97–108.
[5] A. Gupta, G. Upadhya, Optimization of heat pipe wick structures for low wattage electronics cooling applications, Pacific RIM/ASME International Intersociety Electronics Photonic Packaging Conference 'Advances in Electronic Packaging 1999', Sponsored by: ASME, ASME, NY, 1999, pp. 2129–2137.
[6] S.W. Chi, Heat Pipe Theory and Practice, Hemisphere Publishing Corporation, Washington, DC, 1976, Chapters 2 and 3.
[7] F.A.L. Dullien, in: Pourous Media, Transport and Pore Structure, second ed., Academic Press Inc., San Diego, 1992, p. 73.
[8] D.K. Harris, D.R. Cahela, B.J. Tatarchuk, Wet layup and sintering of metal-containing microfibrous composites for chemical processing opportunities, Compos.—Part A: Appl. Sci. Manufact. 32 (8) (2001) 1117–1126.
[9] D.R. Adkins, T.A. Moss, C.E. Andraka, N.H. Andreas, H.M. Cole, An examination of metal felt wicks for heat-pipe applications, in: Proceedings of the 1995 ASME/JSME/JSES International Solar Energy Conference, Sponsored by: ASME, JSME, and JSES, ASME, NY, 1995, pp. 553–558.
[10] C.C. Silverstein, Design and Technology of Heat Pipes for Cooling and Exchange, Hemisphere Publishing Corporation, Washington, DC, 1992, Chapters 2 and 3.
[11] D.A. Pruzan, L.K. Klingensmith, K.E. Torrance, C.T. Avedisian, Design of high-performance sintered-wick heat pipes, Int. J. Heat Mass Transfer 34 (6) (1991) 1417–1427.
[12] D.A. Pruzan, K.E. Torrance, C.T. Avedisian, Two-phase flow and dryout in a screen wick saturated with a fluid mixture, Int. J. Heat Mass Transfer 33 (4) (1990) 673–681.
[13] R.R. Williams, D.K. Harris, Cross-plane and in-plane porous properties measurements of thin metal felts: applications in heat pipes, Exp. Thermal Fluid Sci. 27 (2003) 227–235.
[14] P.D. Dunn, D.A. Reay, Heat Pipes, fourth ed., Elsevier Science Inc., Tarrytown, NY, 1994, Chapters 2 and 3.
[15] Y. Ikeda, Effective thermal conductivity of screen wicks, in: Proceedings of the 1988 National Heat Transfer Conference, Sponsored by: ASME, Heat Transfer Div, ASME, NY, 1988, pp. 717–722.
[16] G.P. Peterson, L.S. Fletcher, Effective thermal conductivity of sintered heat pipe wicks, J. Thermophys. 1 (4) (1987) 343–347.
[17] Y.K. Gontarev, Y.V. Navruzov, V.F. Prisnyakov, V.N. Serebryanskii, Mechanism for boiling of a liquid in heat pipe wicks, J. Eng. Phys. 47 (3) (1984) 1056–1060.
[18] M. O-uchi, M. Izumi, N. Yamakawa, M. Saka, T. Takeyama, Boiling heat transfer of a liquid film formed in the evaporator of a two-phase closed thermosiphon: Part 2, Heat Transfer—Japanese Res. 19 (5) (1990) 429–441.
[19] H.C. Chebaro, K.P. Hallinan, S.J. Kim, W.S. Chang, Evaporation from a porous wick heat pipe for isothermal interfacial, in: Winter Annual Meeting of the American Society of Mechanical Engineers, Sponsored by: ASME, ASME, NY, 1992, pp. 23–28.
[20] V.P. Carey, Liquid–Vapor Phase-change Phenomena, Hemisphere Publishing Corporation, Washington, DC, 1992, Chapter 7.
[21] V.P. Carey, Liquid–Vapor Phase-change Phenomena, Hemisphere Publishing Corporation, Washington, DC, 1992, Chapter 6.
[22] J.J. Lorenz, B.B. Mikic, W.M. Rohsenow, Effect of surface conditions on boiling characteristics, in: Proceeding of the 5th International Heat Transfer Conference, Japanese Society of Mechanical Engineers, 1974, pp. 35–39.
[23] J.H. Rosenfeld, Nucleate boiling heat transfer in porous wick structures, in: Proceedings, Heat Transfer Equipment Fundamentals, Design, Applications, and Operating Problems, Sponsored by: ASME, Heat Transfer Div, Detroit, MI, 1989, pp. 47–55.
[24] L.L. Vasil'yev, S.V. Konev, V.M. Khaustov, Boiling heat transfer on a horizontal pipe with a wick-covered surface, Heat Transfer—Sov. Res. 23 (1) (1991) 117–123.
[25] H. Noda, K. Yoshioka, T. Hamatake, A model for the heat transfer limit of a screen wick heat pipe, Heat Transfer—Japanese Res. 18 (3) (1989) 44–57.
[26] G.E. McCreery, Liquid flow and vapor formation phenomena in a flat heat pipe, Heat Transfer Eng. 15 (4) (1994) 33–41.
[27] R.R. Williams, An investigation of the use of step-graded metal felt wicks to improve heat pipe performance, PhD thesis, Auburn University, Auburn, AL, 2002.
[28] MIL-F-495E, Finish, Chemical, Black, for Copper Alloys, Military Specification, 1988.

[29] A.W. Adamson, Physical Chemistry of Surfaces, Fifth ed., John Wiley and Sons, Inc., New York, 1990.
[30] M.P. Mughal, O.A. Plumb, Experimental study of boiling on a wicked surface, Int. J. Heat Mass Transfer 39 (4) (1996) 771–777.
[31] R.A. Moss, A.J. Kelly, Neutron radiographic study of limiting planar heat pipe performance, Int. J. Heat Mass Transfer 13 (1970) 491–502.
[32] S.H. Moon, C.G. Choi, G. Hwang, T.G. Choy, Experimental study on performance of a miniature heat pipe with woven-wired wick, in: Proceedings of the Intersociety Conference, ITherm 2000, vol. 2, 2000, pp. 129–133.
[33] N.H. Afgan, L.A. Jovic, S.A. Kovalev, V.A. Lenykov, Boiling heat transfer from surfaces with porous layers, Int. J. Heat Mass Transfer 28 (2) (1985) 415–422.